The Baryon Fractions and Mass-to-Light Ratios of Early-Type Galaxies

Guangfei Jiang and C.S. Kochanek

Department of Astronomy, The Ohio State University, Columbus, OH 43210

ABSTRACT

We jointly model 22 early-type gravitational lens galaxies with stellar dynamical measurements using standard CDM halo models. The sample is inhomogeneous in both its mass distributions and the evolution of its stellar populations unless the true uncertainties are significantly larger than the reported measurement errors. In general, the individual systems cannot constrain halo models, in the sense that the data poorly constrains the stellar mass fraction of the halo. The ensemble of systems, however, strongly constrains the average stellar mass represented by the visible galaxies to 0.026 ± 0.006 of the halo mass if we neglect adiabatic compression, rising to 0.056 ± 0.011 of the halo mass if we include adiabatic compression. Both estimates are significantly smaller than the global baryon fraction, corresponding to a star formation efficiency for early-type galaxies of $10\%-30\%$. In the adiabatically compressed models, we find an average local B-band stellar mass-to-light ratio of $(M/L)_0 = (7.2 \pm 0.5)(M_\odot/L_\odot)$ that evolves by $d\log(M/L)/dz = -0.72 \pm 0.08$ per unit redshift. Adjusting the isotropy of the stellar orbits has little effect on the results. The adiabatically compressed models are strongly favored if we impose either local estimates of the mass-to-light ratios of early-type galaxies or the weak lensing measurements for the lens galaxies on 100 kpc scales as model constraints.

Subject headings: early-type galaxies, gravitational lensing, stellar dynamics

1. Introduction

The presence of dark matter in early type galaxies is clear on large scales, based on both weak lensing (e.g. Kleinheinrich et al. 2006, Mandelbaum et al. 2006) and X-ray (e.g. Humphrey et al. 2006) studies. The distribution of the dark matter and the mass fraction represented by the stars are less well-determined because of the difficulties in measuring early-type galaxy structure in the transition region between the stars and the dark matter. Stellar

kinematic studies of the central regions, when compared to estimates of stellar mass-to-light ratios, have argued either that there is little dark matter inside an effective radius (e.g. Gerhard et al. 2001) or that there is a substantial dark matter fraction (e.g. Padmanabhan et al. 2004). The significance of these differences depends on the reliability of estimating the stellar mass from combinations of photometry, spectroscopy and population synthesis models. Studies on larger scales using planetary nebulae, have found examples of galaxies with falling rotation curves (Romanowsky et al. 2003), while the globular clusters in one of these systems show a flat rotation curve (Pierce et al. 2006). Surveys of structure with gravitational lenses (e.g. Rusin & Kochanek 2005, Treu et al. 2006) indicate that the typical lens has a flat rotation curve on scales of 1–$2R_e$, but the interpretation of the scatter around the mean structure has been used to argue for both inhomogeneity (e.g. Treu & Koopmans 2002a, Kochanek et al. 2006) and homogeneity (e.g. Rusin & Kochanek 2005, Koopmans et al. 2006) in the mass distributions.

In this paper we reanalyze a sample of 15 lenses from the Sloan Lens ACS Survey (SLACS, Bolton et al. 2006) and 7 lenses from the Lens Structure and Dynamics Survey (LSD, Koopmans & Treu 2003) that have both mass estimates from the lens geometry and central velocity dispersion measurements. Koopmans et al. (2006) analyzed the sample using a simple, global power law model, $\rho \propto r^{-\gamma}$, for the mass distribution to find a mean slope of $\gamma = 2.01^{+0.02}_{-0.03}$ where $\gamma = 2$ corresponds to a flat rotation curve. With a nominal scatter in the slope of only 0.07, Koopmans et al. (2006) argue that the halo structures appear to be fairly homogeneous. It is difficult, however, to relate these power law models to theoretical models of halos or to evaluate the significance of the scatter in the slope. Additionally, the models are somewhat unphysical because they allow mass distributions more compact that the luminous galaxy.

Here we reanalyze the SLACS and LSD lens samples using a more physical mass model that combines a Hernquist (1990) profile for the stars with a Navarro, Frenk & White (1996, NFW) model for the dark matter. By comparing the mass inside the Einstein ring of the galaxies ($M_E(< R_E)$) with the mass needed to produce the observed velocity dispersion, we can estimate the stellar mass fraction and the stellar mass-to-light ratio explicitly. We use a Bayesian formalism that allows us to quantitatively address the homogeneity of the sample. We review the data and describe our mass models and analysis techniques in §2. In §3, we discuss the models of the individual systems (§3.1), the homogeneity of the sample (§3.2), and finally, the stellar mass fraction, the mean stellar mass-to-light ratio and the evolution of the mass-to-light ratios (§3.3). We summarize our results in §4.

2. Data and Method

2.1. Data

In this paper we reanalyze the data for 15 lenses from the Sloan Lenses ACS Survey (SLACS) and 7 lenses from the Lens Structure and Dynamics Survey (LSD). We neglect two lenses, Q0957+561 and Q2237+030, from the LSD, since Q0957+561 is in a cluster and Q2237+030 is a barred spiral galaxy, to leave us with a sample of 22 galaxies with measured velocity dispersions, effective radii, Einstein radii, enclosed masses and rest frame B band magnitudes taken from the original analyses. For convenience, we summarize the data in Table 1, particularly since the equivalent table in Treu et al. (2006) contains ordering errors. For consistency we have adjusted all the data to a flat ΛCDM cosmological model with $\Omega_m = 0.3$, $\Omega_\Lambda = 0.7$ and $H_0 = 70$ km s^{-1} Myr^{-1}.

2.2. Method of Analysis

We model the lenses with the two component mass model for lenses introduced by Keeton (2001), which was also used for early-type galaxies in the SDSS by Padmanabhan et al. (2004). It consists of a Hernquist (1990) model for the luminous galaxy and a Navarro, Frenk & White (1996, NFW) profile for the dark matter halo. By using this physically motivated model rather than the simple power law normally used by the LSD/SLACS studies, we both better connect the results to theoretical halo models, and avoid models in which the dark matter can be more centrally concentrated than the stars. In essence, we use the mass enclosed by the Einstein radius of the lens to set the virial mass M_{vir}, the stellar velocity dispersion to determine the stellar mass fraction f_*, and theoretical halo models to constrain the halo concentration c. Finally, by comparing the derived stellar mass to the observed luminosity, we can estimate the rest frame B-band mass-to-light ratio M_*/L and its evolution.

The Hernquist (1990) model used for the luminous lens galaxy is defined by

$$\rho_H(r) = \frac{M_*}{2\pi} \frac{r_H}{r(r + r_H)^3},$$ (1)

where the scale length $r_H = 0.551 R_e$ is matched to the measured de Vaucouleurs profile effective radius R_e and the stellar mass $M_* = f_* M_{vir}$ is related to the virial mass by the cold baryon/stellar mass fraction f_*. The NFW profile (Navarro, Frenk & White 1996) used to model the initial dark matter halo is defined by

$$\rho_N(r) = \frac{M_{dm}}{4\pi f(c)} \frac{1}{r(r + r_s)^3},$$ (2)

where the scale length r_s is related to the virial radius by $c = r_{vir}/r_s$, $f(c) = \ln(1 + c) - c/(1 + c)$, and $M_{dm} = (1 - f_*)M_{vir}$ is the mass in dark matter. The average concentration was modeled by

$$c = \frac{9}{1 + z} \left(\frac{M_{vir}}{8.12 \times 10^{12} \ hM_\odot} \right)^{-0.14}, \tag{3}$$

and the individual halos have a log-normal dispersion in their concentrations of $\sigma_c = 0.18$ (base 10) around the average (Bullock et al. 2001). These initial models neglect the compression of the dark matter density profile by the more concentrated baryons. We estimated the changes in the dark matter distribution using the adiabatic compression model of Blumenthal et al. (1986). This approximation may exaggerate the compression (Gnedin et al. 2004), so we should regard our compressed and uncompressed results as bounding the possible effects of adiabatic compression.

The observations provide two constraints, the mass inside the Einstein radius, and the stellar velocity dispersion. For any value of c and f_*, we use the projected mass inside the Einstein radius to determine M_{vir} (which also determines r_{vir}), then use the spherical Jeans equation and a constant orbital isotropy β to compute the velocity dispersion expected for the measurement aperture. The effects of seeing were modeled using a Gaussian PSF with the observed FWHM of the observations. Given the estimated dispersion $\sigma_{i,model}$, the measured dispersion σ_i and its uncertainties $e_{\sigma i}$ for galaxy i, we estimate a goodness of fit $\chi_i^2(\sigma_i) = (\sigma_{i,model} - \sigma_i)^2/e_{\sigma i}^2$. We model the mass-to-light ratios of the stars using the standard power law (e.g. van Dokkum & Franx 1996; Treu 2001; Rusin & Kochanek 2005; Koopmans et al. 2006),

$$\log \left(\frac{M_*}{L} \right) = \log \left(\frac{M_*}{L} \right)_0 + z \left(\frac{d \log(M_*/L)}{dz} \right) \tag{4}$$

where $(M_*/L)_0$ is the value today and $d \log(M_*/L)/dz$ is the rate at which it changes with redshift z. This in turn defines a goodness of fit $\chi_i^2((M/L)_i)$ with which the model fits the logarithm of the mass-to-light ratio $(M/L)_i$ of galaxy i, defined by the ratio of the estimated stellar mass (a model parameter) to the observed luminosity, given its uncertainties $e_{Li} = \Delta(\log(M/L)_i = \Delta L_i/(\ln(10)L_i)$. These two terms define a probability of fitting the velocity dispersion $P(\sigma_i|\xi) = \exp(-\chi_i^2(\sigma_i)/2)/\sqrt{2\pi}e_{\sigma i}$ and the mass-to-light ratio $P((M/L)_i|\xi) = \exp(-\chi_i^2((M/L)_i)/2)/\sqrt{2\pi}e_{Li}$ given the model parameters f_*, c, $(M_*/L)_0$ and $d \log(M/L)/dz$ which we abbreviate as ξ. Combining the two terms, we have the probability of the model fitting the data D_i for galaxy i

$$P_i (D_i|\xi) = P (\sigma_i|\xi) P ((M/L)_i|\xi) . \tag{5}$$

In addition to the measurement errors listed in Table 1, we should also consider sources of systematic errors. The essence of the method is to compare the mass inside the Einstein

ring $M(< R_e)$ to a virial mass estimate from the velocity dispersion $\sigma_v^2 R/G$. We can identify five sources of systematic errors. First, while there is little uncertainty in M_E, some of the mass may be projected surface density from either a parent group halo to which the lens belongs, or from another along the line of sight. The extra density, $\kappa = \Sigma/\Sigma_c$ in dimensionless units, modifies the mass inside the Einstein radius by $\pi\kappa R_E^2 \Sigma_c$, so we can think of its effects as a systematic error in interpreting σ_v of $e_\sigma = \sigma_\kappa/2$. The full probability distribution of κ is skewed to positive values (e.g. Takada & Hamana 2003), but we will ignore this problem and assume $\sigma_\kappa \simeq 0.05$ since the positive tail of the distribution is associated with detectable objects (galaxies and clusters). This systematic error also affects estimates of the mass-to-light ratios. Second, there are $1 - 10\%$ uncertainties in the galaxy effective radius measurements which contribute uncertainties of 0.5% to 5% to our interpretation of the velocity dispersion. Third, the measured velocity dispersion is a Gaussian fit to the spectrum, which is not identical to the rms velocity appearing in the Jeans equation (e.g. Binney & Tremaine 1987). The difference can be estimated from the typical Gaussian-Hermite coefficients $|h_4| \simeq 0.02$ (Bender, Saglia & Gerhard 1994) as a fractional error in σ_v of order $\sqrt{6}|h_4| \simeq 0.05$ in the velocity dispersion (e.g. van der Marel, van Dokkum & Franx 2003). Fourth, non-sphericity, (somewhat to our surprise) leads to negligible systematic errors provided we use the intermediate scale length (the geometric mean of the semi-major and minor axes), at least in the limit of the tensor virial theorem. It leads to large errors if any other scale length is used. Barnabe & Koopmans (2007) have taken the first steps towards removing these two dynamical problems, although they are restricted to oblate two-integral models which may not be appropriate for massive elliptical galaxies. Finally, calibration errors in the velocity dispersions contribute fractional errors of order 0.03 (see Bernardi et al. 2003a). Combining all these contributions in quadrature, which corresponds to assuming a Gaussian model for each systematic error, we estimate that the typical systematic uncertainty to interpreting the velocity dispersions is approximately 8% with the exact value depending on the uncertainties in the effective radius.

Our statistical methods are chosen so that we can understand the homogeneity of the lens galaxies in either their evolution or their dynamical properties and estimate their average properties in the presence of inhomogeneities. We will analyze the results using two Bayesian methods. In the first method, we will fit the data while simultaneously estimating the systematic errors in the velocity dispersion and the mass-to-light ratio. When combined with the measurement errors, these define new uncertainty estimates for the data which we will call the "bad" case errors in comparison to the original uncertainties (the "good" case). These broadened uncertainties can be representative of either true systematic uncertainties, such as the ones we discussed above for the dynamical measurements, or indicative of inhomogeneities in the structure or evolution of the galaxies. In the second method we will compare these two

cases using the approach outlined in Press (1997) to determine the degree to which the sample homogeneous or heterogeneous. In this method, we assume that there are probabilities p_σ and p_L that the galaxies have homogeneous structures or evolutionary histories in the sense that the scatter in the measurements is simply determined by the "good" measurement errors. There are then probabilities $1 - p_\sigma$ and $1 - p_L$ that the galaxies are not a homogeneous group in either their structure or their evolution, where we characterize this by assuming that the uncertainties in the velocity dispersion and the mass-to-light ratio are significantly broadened to be the "bad" measurement errors. In essence, we are determining the relative probabilities of the stated measurement errors and our estimate of the true uncertainties from the first method. Both approaches provide uncertainties on the average properties of the sample that account for potential inhomogeneities, although the second method is a better formal approach since it can reject individual objects.

In the first approach, we will estimate the fractional systematic errors e_σ and e_L in the velocity dispersion and luminosity. The χ^2 expressions are modified to use uncertainties of $e_{\sigma i} \rightarrow \sqrt{e_{\sigma i}^2 + e_\sigma^2 \sigma_i^2}$ and $e_{Li} \rightarrow \sqrt{e_{Li}^2 + e_L^2}$ for the velocity dispersions and the logarithm of the mass-to-light ratios respectively. We assume logarithmic priors for f_*, $(M_*/L)_0$, and $(d(M/L)/dz)$, and the theoretical prior defined by Eqn. (3) for the concentration c_i. Note that we are forcing all galaxies to have the same concentration, which should have no significant impact given the scales we are studying. The priors for the systematic errors, $P(e_\sigma) = 1/\sqrt{\langle e_{\sigma i}^2 \rangle + e_\sigma^2 \sigma_i^2}$ and $P(e_L) = 1/\sqrt{\langle e_{Li}^2 \rangle + e_L^2}$, naturally switch between uniform priors for systematic errors small compared to the mean square measurement errors ($\langle e_{\sigma i}^2 \rangle$ and $\langle e_{Li}^2 \rangle$) and logarithmic priors for large systematic errors. The resulting probability distribution for the fractional errors is then

$$P(e_\sigma, e_L | D) \propto P(e_\sigma) P(e_L) \int d\xi P(\xi) \prod_i P(D_i | e_\sigma, \xi) P(D_i | e_L, \xi) \qquad (6)$$

where $P(D_i | e_\sigma, \xi)$ and $P(D_i | e_L, \xi)$ are the probability distributions modified by the addition of the systematic errors e_σ and e_L. We then use these systematic error estimates to define the uncertainties used for the "bad" case in our second formalism.

The second, Press (1997) approach properly weights all combinatoric possibilities of the individual systems being members of a homogeneous sample or not. Let $P_{Gi}(\sigma_i | \xi)$ and $P_{Gi}((M/L)_i | \xi)$ be the probabilities of the data given the parameters for galaxy i if it is a member of a homogeneous group based on the measured, "good" uncertainties, and $P_{Bi}(\sigma_i | \xi)$ and $P_{Bi}((M/L)_i | \xi)$ be the probabilities if it is not and we should be using the "bad" uncertainties based on the systematic error estimates derived from our first method. The Press (1997) provides estimates of the relative likelihoods describing either the full sample or the individual systems by the "good" or "bad" data model. If we want the Bayesian probabil-

ity distribution for the parameters ξ properly weighted over all possible group membership combinations, we find that

$$P(\xi|D) \propto P(\xi) \int dp_\sigma dp_L \prod_i F_i \qquad (7)$$

where

$$F_i = [p_\sigma P_{Gi}(\sigma_i|\xi) + (1 - p_\sigma)P_{Bi}(\sigma_i|\xi)] \, [p_L P_{Gi}((M/L)_i|\xi) + (1 - p_L)P_{Bi}((M/L)_i|\xi)] \qquad (8)$$

and where $P(\xi)$ sets the prior probability distributions for the parameters. We assume a uniform priors for p_σ and p_L. We obtain the probability distribution for any parameter by marginalizing Eqn. (7) over all other variables and then normalizing the total probability to unity. We can also estimate the probability that the sample is homogeneous in either its structural or evolutionary properties as

$$P(p_\sigma, p_L|D_i) \propto \int d\xi P(\xi)\Pi_i F_i \qquad (9)$$

and the probability that a particular galaxy is in the dynamically homogeneous class is

$$P(\sigma_i \in \text{homogeneous}|D) = \frac{A_i}{A_i + B_i} \qquad (10)$$

where

$$A_i = \int d\xi P(\xi) \int dp_\sigma dp_L p_\sigma P_{Gi}(\sigma_i) \, [p_L P_{Gi}((M/L)_i|\xi) + (1 - p_L)P_{Bi}((M/L)_i|\xi)] \, \Pi_{i \neq j} F_j \quad \text{and} \quad (11)$$

$$B_i = \int d\xi P(\xi) \int dp_\sigma dp_L (1 - p_\sigma)P_{Bi}(\sigma_i) \, [p_L P_{Gi}((M/L)_i|\xi) + (1 - p_L)P_{Bi}((M/L)_i|\xi)] \, \Pi_{i \neq j} F_j.$$

A similar set of expressions gives the probability that the galaxy is in the set of galaxies with a homogeneous evolutionary history.

3. Results

We divide our discussion of the results into three subsections. First, we present the results for the individual galaxies. Next, we discuss the homogeneity of the structural properties of the galaxies. Finally, we estimate the stellar mass fraction, mass-to-light ratios and the rate of galaxy evolution.

3.1. Properties of Individual Galaxies

Figure 1 shows contours for the goodness of fit of the models to the velocity dispersion, measured for each galaxy as a function of the stellar mass fraction f_* and the concentration c once we have normalized the mass inside the Einstein radius. For these calculations, we have included our estimates of the systematic errors in the velocity dispersions but used the stated uncertainties in the luminosities. Note that the dispersion measurements cannot determine the halo concentrations but the goodness of fit contours always pass through the region set by our prior on the concentration. The permitted stellar mass fractions vary widely between objects. Three of the 22 objects, SDSS $J0737 + 321$, SDSS $J1250 + 052$ and PG1115 + 080, appear to require mass distributions that are more centrally concentrated than the stars, in the sense that the best fits for $f_* \leq 1$ have $\chi^2 > 2$. This is also seen in the LSD models for PG1115 + 080 (Treu & Koopmans 2002a), where the only models consistent with both the lensing constraint and the estimated velocity dispersion are more centrally concentrated than the stars. A fourth lens, SDSS $J1627-005$, is only marginally consistent with $f_* \leqslant 1$. Of the remaining 18 galaxies, eleven are consistent with $f_* = 1$ ($\Delta\chi^2 < 1$), and seven are not. Four of these eleven galaxies have enormous parameter uncertainties. One problem for many SLACS lenses is that the scales of the velocity dispersion aperture/effective radius differ little from the observed Einstein radius, which limits the leverage for constraining the mass profile.

Figure 2 shows the goodness of fit to the mass-to-light ratio of each galaxy given the best fit model for the average evolution of the sample. Most of the galaxies are consistent with this best fit model for the mass-to-light ratio and its evolution (§3.3). The mass-to-light ratios of the sample appear to be more uniform than the dynamical properties, probably for the same reasons that there is little scatter in the fundamental plane (see Bernardi et al. 2003b). However, there are three 3σ outliers in the sample, SDSS J1420+602, SDSS J1250+052 and H1543+535, all of which have very low M/L ratios compared to the other galaxies. Note that only one of these, SDSS J1250+052, is also an outlier in the dynamical fits. This is not unique to our approach, since our mass-to-light ratio for H1543+535 is comparable to that in Treu & Koopmans (2004). In Figure 6 of Treu et al. (2006), they also find significantly lower mass-to-light ratios for SDSS J1420+602 and SDSS J1250+052 than they do for the other SLACS members. One possible solution is that the lens masses are significantly mis-estimated due to contamination from a group or cluster halo, but only H1543+535 has a neighboring, bright galaxy and it is sufficiently distant to only modestly perturb the estimated mass.

3.2. Homogeneity

The broad uncertainties and occasional outliers mean that it is important to have a quantitative approach to determining the homogeneity of the sample and to appropriately weight each object when determining mean properties. This is why we introduced the Bayesian frameworks of §2. Fig. 3 shows our estimates of the fractional systematic errors from our first analysis method (Eqn. 6). The best fit estimates for the fractional systematic errors in the velocity dispersion and luminosity are $e_\sigma \simeq 0.1$ and $e_L \simeq 0.18$. The reported measurement errors lie well outside the 99.7% likelihood region. For the dynamical errors, the best fit systematic errors are quite consistent with our prior estimates based on simple considerations about the dynamical data.

Fig. 4 shows that the results for the homogeneity of the sample are very sensitive to the assumed uncertainties. If we simply used the stated measurement errors, then the probability that the sample is homogeneous in its dynamical properties (i.e. that the "good" uncertainty estimates are correct and the scatter is due only to measurement error) is $p_\sigma \leq 24\%$ and that it is homogeneous in mass-to-light ratio evolution is $p_L \leq 14\%$. Many objects have low probabilities of belonging to either a homogeneous dynamical subset (SDSS J1627–0053 with $p_\sigma = 0.005$, SDSS J1250+0523 with $p_\sigma = 0.010$, SDSS J0737+321 with $p_\sigma = 0.010$, PG1115+080 with $p_\sigma = 0.029$, and SDSS J1420+602 with $p_\sigma = 0.042$) or a homogeneous evolutionary subset (SDSS J1250+0523 $p_L \approx 0$, H1543+535 $p_L \approx 0$, SDSS J0912+002 $p_L = 0.001$, SDSS J1420+602 $p_L = 0.001$ and MG1549+305 $p_L = 0.001$). Not surprisingly, these objects are also outliers in the individual fits from the previous section. If we include our estimates of the systematic errors in interpreting the dynamical measurements, then the probability that the sample is homogeneous in its dynamical properties rises to $p_\sigma \geq 40\%$, but the probability of a homogeneous evolutionary population remains small at $p_L \leq 14\%$. With the inclusion of the systematic error estimates, the objects with the lowest probabilities of belonging to the homogeneous dynamical subset are PG1115+080 (with $p_\sigma = 0.48$), SDSS J1250+0523 (with $p_\sigma = 0.49$), SDSS J1627–0053 (with $p_\sigma = 0.52$), SDSS J0737+321 (with $p_\sigma = 0.52$), and H1417+526 (with $p_\sigma = 0.55$). These estimates strongly indicate that either the SLACS/LDS lens populations are inhomogeneous or that the measurement errors underestimate the true uncertainties. In a few cases, these problematic lenses show some evidence for disks (SDSS J1420+602, MG1549+305).

In sum, the SLACS/LDS galaxies are homogeneous in neither their dynamical nor their evolutionary properties if we take the measurement errors at face value. It is likely that most of the problem for the dynamical measurements is that the systematic errors in interpreting velocity dispersions are significant and need to be included in any analysis of the dynamics of lenses. One of these systematic errors, surface density contributions from structures

other than the lens galaxy, also produces systematic errors in the mass-to-light ratio, with $\sigma_M = \sigma_\kappa \simeq 0.05$, but this is much too small to explain the spread in the mass-to-light ratios. This problem is probably caused by a combination of underestimated uncertainties in the luminosities and true variance in the evolutionary history of early-type galaxies. Rusin & Kochanek (2005) and Treu et al. (2006) had found earlier that the lens sample was better fit by allowing a range for the mean redshift at which the stars formed than by assuming a single value, and in this analysis a range of formation redshifts would lead to non-zero systematic errors in the mass-to-light ratio.

3.3.   The Stellar Mass Fraction and Mass-to-Light Ratio

We can combine the galaxies to make joint estimates of the stellar mass fraction f_*, the mass-to-light ratio M_*/L at $z = 0$ and its evolution. We considered both Bayesian frameworks so that either the uncertainties are broadened to make the results consistent with all the lenses (method 1, Eqn. 6) or the outliers in the sample are properly down weighted in the analysis (method 2, Eqn. 7) The two methods give similar results, so we only present the detailed results from the second Bayesian method. Fig. 5, shows the estimated stellar mass fraction f_* for both the individual galaxies and the sample as a whole, and for orbital anisotropies of $\beta = -1/3, 0$ and $1/3$, where $\beta = 1 - \sigma_t^2/\sigma_r^2$ is related to the ratio of the tangential σ_t and radial σ_r velocity dispersions. For isotropic, adiabatically compressed models, we find $f_* = 0.056 \pm 0.011$, and like Koopmans et al. (2006), we find that that the isotropy has little effect on the inferred mass distribution. The stellar mass fraction is significantly lower than the global baryon fraction of $0.176^{+0.006}_{-0.019}$ from the WMAP CMB anisotropy measurements (Spergel et al. 2006). If we do not include the adiabatic compression of the halo, the stellar mass fraction drops to 0.026 ± 0.006, again with little dependence on the isotropy β. While the uncompressed models have less dark matter in the central regions, the total halo mass is much larger than in the compressed models. To the extent that adiabatic compression occurs, but the Blumenthal et al. (1986) model exaggerates its degree (Gnedin et al. 2004), reality is intermediate to these two extremes.

We also fit the mass-to-light ratio as $\log(M_*/L) = \log a + bz$, where $a = (M_*/L)_0$ is the mass-to-light ratio at $z = 0$ and $b = d(\log(M_*/L))/dz$ is its evolution with redshift. Fig. 6, shows the likelihood contours for these two parameters for both compressed and uncompressed models. For the compressed isotropic models, we find $a = (7.2 \pm 0.5)M_\odot/L_\odot$ and $b = -0.72 \pm 0.08$. This agrees with the local value of $a = (7.3 \pm 2.1)M_\odot/L_\odot$ from Gerhard et al. (2001) that was used by Treu et al. (2006). It also agrees with the Treu et al. (2006) estimate for the rate of the evolution $b = -0.69 \pm 0.08$. Changing the isotropy over

the range $\beta = -1/3, 0, 1/3$ has little effect, while the model without adiabatic compression requires higher normalizations for the mass-to-light ratio (10.0 ± 0.3) and slightly slower rates of evolution. Our analysis includes 2 lenses (PG1115+080 and H1543+535) that were not used by Treu et al. (2006), but excluding them from the analysis has little effect on the mass-to-light ratios. There are no significant changes in $(M_*/L)_0$ and $d\log(M_*/L)/dz$ if we neglect these two lenses.

4. Discussion

We reanalyzed the data from the SLACS and LSD surveys of gravitational lenses with velocity dispersion measurements. Our mass distribution consists of a Hernquist model for the luminous galaxy embedded in a theoretically constrained NFW halo model. We investigated the homogeneity of the sample, the stellar mass fraction f_*, the local $(z = 0)$ stellar mass-to-light ratio $(M_*/L)_0$ and its evolution $d(\log(M_*/L))/dz$. As in the earlier study by Koopmans et al. (2006), we found that the effects of orbital anisotropy on both the stellar mass fraction and the mass-to-light ratio are small.

In most cases, a central velocity dispersion measurement provides only weak a constraint on halo structure in the physically interesting region. Typical limits on the mass fraction represented by the stars have logarithmic errors of order 0.5 dex. While this appears to contradict the conclusions of (for example) Koopmans et al. (2006), this is not the case. Koopmans et al. (2006) fit mass models where $\rho \propto r^{-\gamma}$, and find values in the range $1.8 < \gamma < 2.3$. Fig. 7 shows the expected range of this slope for our models of SDSS J0037–0942, where we estimated the slope by fitting the $\rho \propto r^{-\gamma}$ power law model to the projected mass distribution over a radial baseline of $R_e/8$ to R_E that approximates the leverage in using stellar dynamics combined with gravitational lensing to determine halo structure. For this typical lens, the variations in γ of $1.6 \lesssim \gamma \lesssim 2.06$ are comparable to the system-to-system spread in γ observed for the SLACS systems (Koopmans et al. (2006)). Thus, the spread in γ observed for individual SLACS/LSD lenses is comparable to the range of values found in our halo models, so strong conclusions about halo structure from these system will depend on averages over the samples rather than the results for individual lenses.

The critical issue for determining the sample average properties is the degree to which the populations are homogeneous. A heterogeneous sample cannot easily be averaged to determine mean properties. We find the probability of homogeneity is very sensitive to the uncertainties in both the velocity dispersion and the luminosity. If take the measurement errors at face value, there is a low probability of homogeneity in either dynamical structure $(p_\sigma \leq 20\%)$ or evolutionary history $(p_L \leq 15\%)$. Many lenses such as SDSS J1250+052,

H1543+535, SDSS J1420+601, SDSS J0912+002, MG2016+112, and MG1549+305 have low ($< 10\%$) likelihoods of belonging to a homogeneous sample. The primary problem is probably that there are significant systematic uncertainties that must be included with the measurement errors. Simple considerations show that typical systematic errors in interpreting the velocity dispersions should be large compared to the measurement errors, 8% versus 5%, and adding these estimated systematic uncertainties greatly increases the likelihood of dynamical homogeneity. Sources of systematic error in the mass-to-light ratio are less amenable to simple arguments, but should certainly include the dispersion in the average star formation epoch of early-type galaxies found in an earlier analyses of galaxy evolution with lenses by Rusin & Kochanek (2005) and Treu et al. (2006). If we simply analyze the data to determine the most likely systematic errors, we find that we must include fractional systematic errors of approximately 10% in the velocity dispersion estimates and 19% in the mass-to-light ratio estimates in order to make the sample consistent with the hypothesis of homogeneity.

Once we account for the inhomogeneity or systematic errors in the sample, we can evaluate sample averages that properly account for these problems. We find that the halo mass fraction represented by the baryons in stars is $f_* = 0.056 \pm 0.011$ if we adiabatically compress the dark matter and $f_* = 0.026 \pm 0.006$ if we do not. These results are comparable to similar the range of estimates that relied on stellar population models to estimate the stellar mass. For example, Lintott, Ferreras & Lahav (2006) obtained a stellar mass fraction of $\backsim 8\%$ by fitting monolithic collapse models to 2000 SDSS galaxies, Hoekstra et al. (2005) found $f_* = 0.065^{+0.010}_{-0.008}$ using weak lensing, and Mandelbaum et al. (2006) found $f_* = 0.03^{+0.02}_{-0.01}\%$ using weak lensing. The results in these studies depend on the assumed IMF – the Hoekstra et al. (2005) estimate drops to $f_* = 0.035^{+0.005}_{-0.004}$ if the initial mass fraction of the stars is changed from a standard Salpeter IMF to a scaled Salpeter IMF. Our results probably bound the stellar mass fraction since the Blumenthal et al. (1986) model we used may overestimate the amount of adiabatic compression (Gnedin et al. 2004). In all our models, the stellar mass fraction is much smaller than the cosmological baryon mass fraction $\Omega_b/\Omega_m = 0.176^{+0.006}_{-0.019}$ from WMAP (Spergel et al. 2006), which means that the star formation efficiency ($f_*\Omega_m/\Omega_b$) of early-type galaxies is only 15–30%. The remaining baryons must remain as gas distributed on the scale of the halo or its parent (group) halo. This discrepancy appears to be a common problem for any baryon accounting for normal galaxies (e.g. Fukugita 2004) and a significant constraint on star formation efficiency.

Analysis of the evolution of early-type galaxies with redshift, whether using the fundamental plane (e.g. Jørgensen et al. 1999; Franx et al. 2000; Treu et al. 2006), dynamical mass estimates (e.g. van der Marel & van Dokkum 2006), or gravitational lens data alone (e.g. Rusin & Kochanek 2005), have consistently observed a steady brightening of early-

type galaxies with look-back time, albeit with modest disagreements as to the rate. Here we use a hybrid method, fitting the stellar mass-to-light ratios inferred from mass models of gravitational lenses with stellar dynamical data, to find that $(M_*/L)_0 = (7.2 \pm 0.5)M_\odot/L_\odot$ and $d(\log(M_*/L))/dz = -0.72 \pm 0.08$ for the compressed models. The mass-to-light ratio is comparable to the local value of $(M_*/L)_0 = (7.3 \pm 2.1)M_\odot/L_\odot$ from Gerhard et al. (2001) which was adopted by Treu et al. (2006) in their analysis of this data. The mass-to-light ratio evolution rate is also close to the value $d\log(M_*/L)/dz = 0.69 \pm 0.08$ from Treu et al. (2006), and marginally larger than the estimates by Rusin & Kochanek (2005) and van der Marel & van Dokkum (2006). As pointed out by Rusin & Kochanek (2005), the differences in evolution rates are partly due to different approaches to weighting the contribution of each lens to the analysis, but at least our Bayesian approach carries out these weightings in an objective fashion.

In our basic analysis we cannot distinguish between the adiabatically compressed and uncompressed models. In essence, we can obtain the same mass distribution either using a high stellar mass-to-light ratio and a more extended halo or the reverse. If we impose the locally estimated mass-to-light ratio as a constraint, then the adiabatically compressed model is favored (6 to 1). We can also use mass measurements on much larger scales to distinguish the two models because the total halo mass is larger in the uncompressed model. In particular, we can calculate the weak lensing $\Delta\Sigma$ and compare it to the measurement by Gavazzi et al. (2007, also see Mandelbaum et al. 2006) for an overlapping sample of SLACS lenses where they found that $\Delta\Sigma = (100 \pm 30)hM_\odot$ pc^{-2} on scales of $94h^{-1}$ kpc. With this constraint the adiabatically compressed models are again strongly favored (by 1000 to 1). In general, any third constraint that is dominated by the contribution from one mass component will break the degeneracy and lead to constraints on the degree of adiabatic compression or an additional structural variable such as the inner slope of the dark matter density distribution.

The sample of lenses available for such analyses will continue to grow and can include lenses with time delay measurements (which constrain the halo structure by measuring the surface density near the lensed images, Kochanek 2002) as well as those with velocity dispersions. With larger samples it should be possible to explore additional correlations such as the scaling of the stellar mass fraction and mass-to-light ratios with halo mass and the dependence of the evolution rate on halo mass. In the Mandelbaum et al. (2006) and Padmanabhan (2004) analyses of early-type galaxies in the SDSS, the changes in the mass-to-light ratio with halo mass are due to an increasing dark matter fraction with mass rather than changes in the stellar populations, but their results depend on population synthesis models to correctly estimate the stellar masses. In a larger sample of lenses, this could be tested directly. van der Marel & van Dokkum (2006) and Treu et al. (2006) see some evi-

dence for differential evolution with mass, but significantly larger samples will be needed to test this given the sensitivity of even the present results to sample weighting.

REFERENCES

Barnabe, M., & Koopmans, L.V.E., 2007, ApJ submitted [astro-ph/0701372]

Bender, R., Saglia, R.P., & Gerhard, O.E., 1999, MNRAS, 269, 785

Bernardi, M., et al., AJ, 2003, 125, 1817

Bernardi, M., et al., AJ, 2003, 125, 1866

Binney, J., & Tremaine, S., 1987, Galactic Dynamics, (Princeton: Princeton Univ. Press), 195

Blumenthal, G., Faber, S., Flores, R., & Primack, J., 1986, ApJ, 301, 27

Bullock, J.S., et al., 2001, MNRAS, 321, 559

Franx, M., 2000, ASPC, 197, 231

Fukugita, M., 2004, IAUS, 220, 227

Gavazzi, R., et al., 2007, astro-ph/0701589

Gerhard, O., et al., AJ, 2001, 121, 1936

Gnedin, O., et al., ApJ, 2004, 616, 16

Hernquist, L., 1990, ApJ, 356, 359

Hoekstra, H., et al., 2005, ApJ, 635, 73

Jørgensen, I., et al., 1999, MNRAS, 197, 231

Keeton, C. R., 2001, ApJ, 561, 46

Keeton, C. R., Kochanek, C. S., & Falco, E. E., 1998, ApJ, 509, 561

Kleinheinrich, M., et al., 2006, A&A, 455, 441

Kochanek, C.S., 2002, ApJ, 578, 25

Koopmans, L. V. E. & Treu, T., 2002, ApJ, 568, L5

Koopmans, L. V. E. & Treu, T., 2003, ApJ, 583, 606

Koopmans, L. V. E., et al. 2006, 649, 599

Lehár, J., et al., 1993, AJ, 105, 847

Lehár, J., et al., 1996, AJ, 111, 1812L

Lintott, C.J., Ferreras, I., & Lahav, O., 2006, ApJ, 648, 826

Mandelbaum, R., Seljak, U., Kauffmann, G., Hirata, C.M., & Brinkmann, J., 2006, MNRAS, 368, 715

Navarro, J.F., Frenk, C.S., & White. S.D.M., 1996, ApJ, 462, 563

Padmanabhan, N., et al., 2004, New Astronomy, Volume 9, Issue 5, 329

Pierce, M., 2006, MNRAS, 366, 1253

Press, W.T., 1997, in Unsolved Problems in Astrophysics, eds. Bahcall, J. N., & Ostriker, J. P., (Princeton: Princeton Univ. Press), 49

Romanowsky, A.J., et al., 2003, Science, 301, 1696

Rusin, D., & Kochanek, C. S., 2005, ApJ, 623, 666

Spergel, D.N., et al., 2006, astro-ph/0603449

Takada, M., Hamana, T., 2003, MNRAS, 346, 949

Tonry, J.L., 1998, AJ, 115, 1

Treu, T., 2001, AAS, 198, 2005T

Treu, T., et al. 2006, ApJ, 640, 662

Treu, T. & Koopmans, L. V. E., 2003, MNRAS, 343L, 29T

Treu, T. & Koopmans, L. V. E., 2004, ApJ, 611, 739

Treu, T. & Koopmans, L. V. E., 2002, MNRAS, 337, L6

Treu, T., et al., 2003, astro-ph/0311052

van Dokkum, P.G., & Franx, M., 1996, MNRAS, 281, 985

van de Ven, G., van Dokkum, P.G., & Franx, M., 2003, MNRAS, 344, 924

van der Marel, R.P. & van Dokkum, P.G., 2006, astro-ph/0611577

Kauffmann, G., 1996, MNRAS, 281, 487

Table 1. Lens data

Objects	z_l	z_s	R_e ($''$)	R_E (kpc)	M_E $(10^{10})M_\odot$	σ_{ap} (km s^{-1})	L_B $(10^{11})L_{B,\odot}$	Aperture ($''$)	seeing ($''$)	$f_{dm}(<R_E)$ compr	$f_{dm}(<R_E)$ nocompr	reference
SDSS J0037−0942	0.1955	0.6322	2.38	4.77	27.3	265±10(30)	1.24±0.11	1.5	1.76	0.42	0.22	1,2
SDSS J0216−0813	0.3317	0.5235	3.37	5.49	48.2	332±23(37)	2.60±0.39	1.5	2.73	0.52	0.35	1,2
SDSS J0737+3216	0.3223	0.5812	3.26	4.83	31.2	310±15(30)	2.13±0.16	1.5	2.33	0.42	0.25	1,2
SDSS J0912+0029	0.1642	0.3240	4.81	4.55	39.6	313±12(29)	1.63±0.20	1.5	1.49	0.50	0.32	1,2
SDSS J0956+5100	0.2405	0.4700	2.60	5.02	37.0	299±16(30)	1.25±0.18	1.5	1.63	0.43	0.24	1,2
SDSS J0959+0410	0.1260	0.5349	1.82	2.25	7.7	212±12(21)	0.27±0.06	1.5	1.58	0.39	0.20	1,2
SDSS J1250+0523	0.2318	0.7950	1.77	4.26	18.9	254±14(25)	1.13±0.06	1.5	1.48	0.36	0.16	1,2
SDSS J1330−0148	0.0808	0.7115	1.23	1.30	3.2	178±9(17)	0.09±0.06	1.5	1.84	0.29	0.10	1,2
SDSS J1402+6321	0.2046	0.4814	3.14	4.66	30.3	275±15(28)	1.06±0.23	1.5	1.83	0.44	0.25	1,2
SDSS J1420+6019	0.0629	0.5352	2.60	1.27	3.9	194±5(17)	0.28±0.09	1.5	2.37	0.33	0.13	1,2
SDSS J1627−0053	0.2076	0.5241	2.14	4.11	22.2	275±12(26)	0.75±0.07	1.5	1.87	0.34	0.15	1,2
SDSS J1630+4520	0.2479	0.7933	2.02	7.03	50.8	260±16(29)	1.15±0.33	1.5	1.52	0.57	0.42	1,2
SDSS J2300+0022	0.2285	0.4635	1.80	4.56	30.4	283±18(30)	0.72±0.13	1.5	1.87	0.40	0.20	1,2
SDSS J2303+1422	0.1553	0.5170	4.20	4.41	27.5	260±15(26)	1.09±0.22	1.5	1.65	0.50	0.32	1,2
SDSS J2321−0939	0.0819	0.5324	4.47	2.43	11.7	236±17(21)	0.76±0.12	1.5	2.09	0.44	0.25	1,2
0047−281	0.484	3.595	0.82	12.43	58.0	250±30(41)	1.20±0.08	1.5×4.3	0.7	0.59	0.44	3,4
C0302+006	0.938	2.941	1.6	10.6	67.0	256±19(31)	3.25±0.45	0.5×1.25	0.8	0.29	0.11	8,9
PG1115+080	0.310	1.722	0.85	4.74	17.0	281±25(36)	0.35±0.02	1.0×1.0	0.8	0.83	0.78	5,6
H1417+526	0.810	3.399	1.06	11.4	70.8	212±18(26)	2.42±0.23	0.32×1.25	0.75	0.62	0.49	9,10
H1543+535	0.497	2.092	0.41	2.4	3.4	108±14(17)	0.28±0.04	0.3×1.25	0.8	0.84	0.78	9
MG1549+305	0.111	1.170	0.82	2.33	12.0	227±18(28)	0.17±0.02	1.0×4.3	0.65	0.60	0.46	11,12
MG2016+112	1.004	3.263	0.31	13.70	110.0	304±27(47)	1.60±0.08	0.65	0.7	0.44	0.26	7

Note. — z_l and z_s are the lens and source redshifts, R_e is the lens effective radius, R_E and M_E are the lens Einstein radius and Einstein mass, σ_{ap} is the measured velocity dispersion. We include both the measurement errors inside the listed aperture and our estimated systematic uncertainties are in (brackets). We lacked the seeing FWHM for SDSS J1627−0053 and SDSS J2300+0022 and simply used the average value for the other SDSS objects. $f_{dm}(<R_E)$ is the projected dark matter fraction inside the Einstein radius for adiabatically compressed ("compr") or not compressed ("no compr") models.

Treu et al. (2006)(1), Koopmans et al. (2006)(2), Treu et al. (2003)(3), Koopmans & Treu (2003)(4)

Tonry (1998)(5), Treu & Koopmans (2002a)(6) , Koopmans & Treu (2002)(7)

Treu & Koopmans (2003)(8), Treu & Koopmans (2004)(9) , Keeton et al. (1998)(10), Lehár et al. (1993)(11)
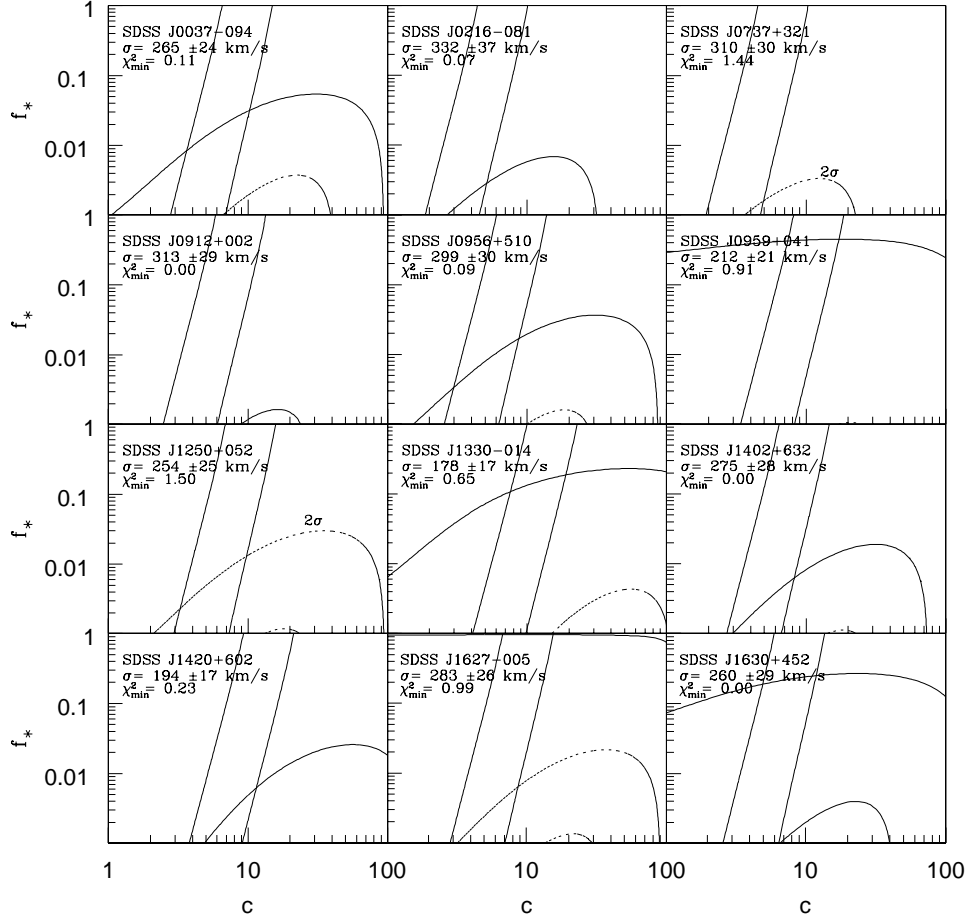
Lehár et al. (1996)(12)

Fig. 1.— The goodness of fit to the velocity dispersion as a function of stellar mass fraction f_* and concentration c. The solid curves are drawn at $\Delta\chi^2 = 1(1\sigma)$ for the fit to the velocity dispersion and the dotted lines are drawn at $\Delta\chi^2 = 4$, 9 and 16 (2, 3, and 4 σ). When there is no region with $\Delta\chi^2 < 1$, we label the lowest contour present. The roughly vertical pair of solid lines indicate the 1σ range of concentrations given the halo mass at each point. The inset text identifies the object, the measured velocity dispersion and the χ^2 of the best fit. These are the isotropic ($\beta = 0$) adiabatically compressed models that include our estimate of the systematic uncertainties in the stellar dynamical measurements.
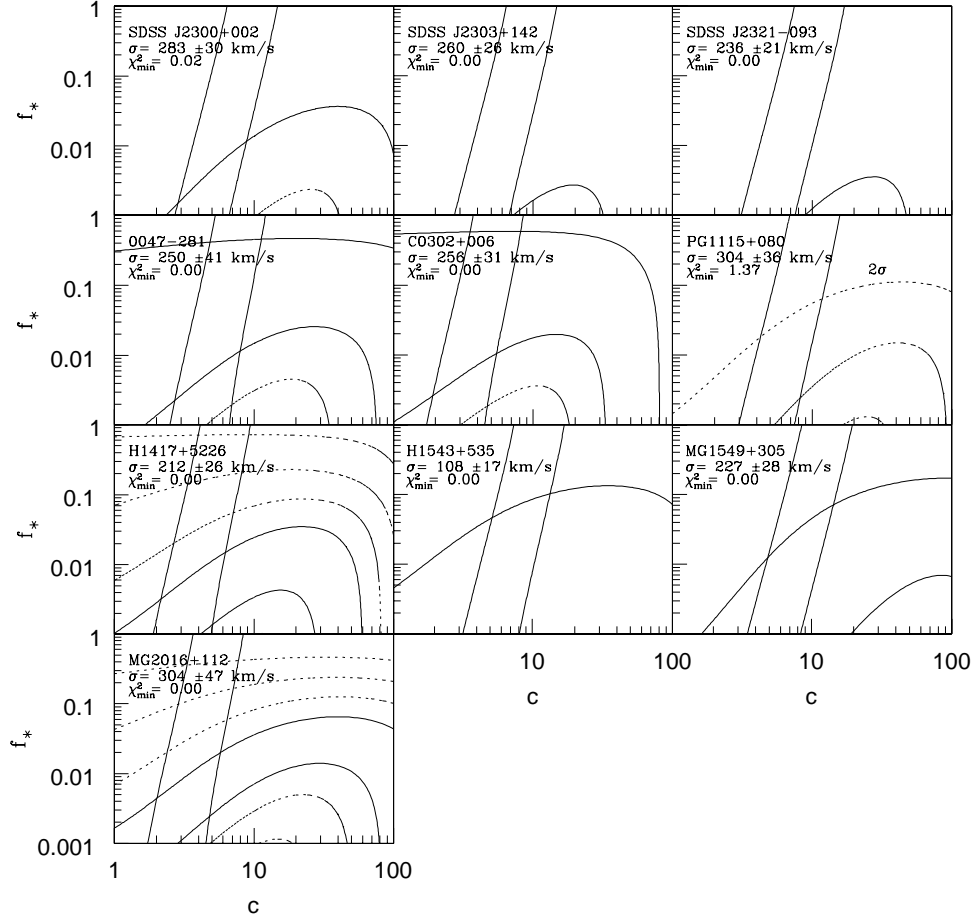
Fig. 1.— continued
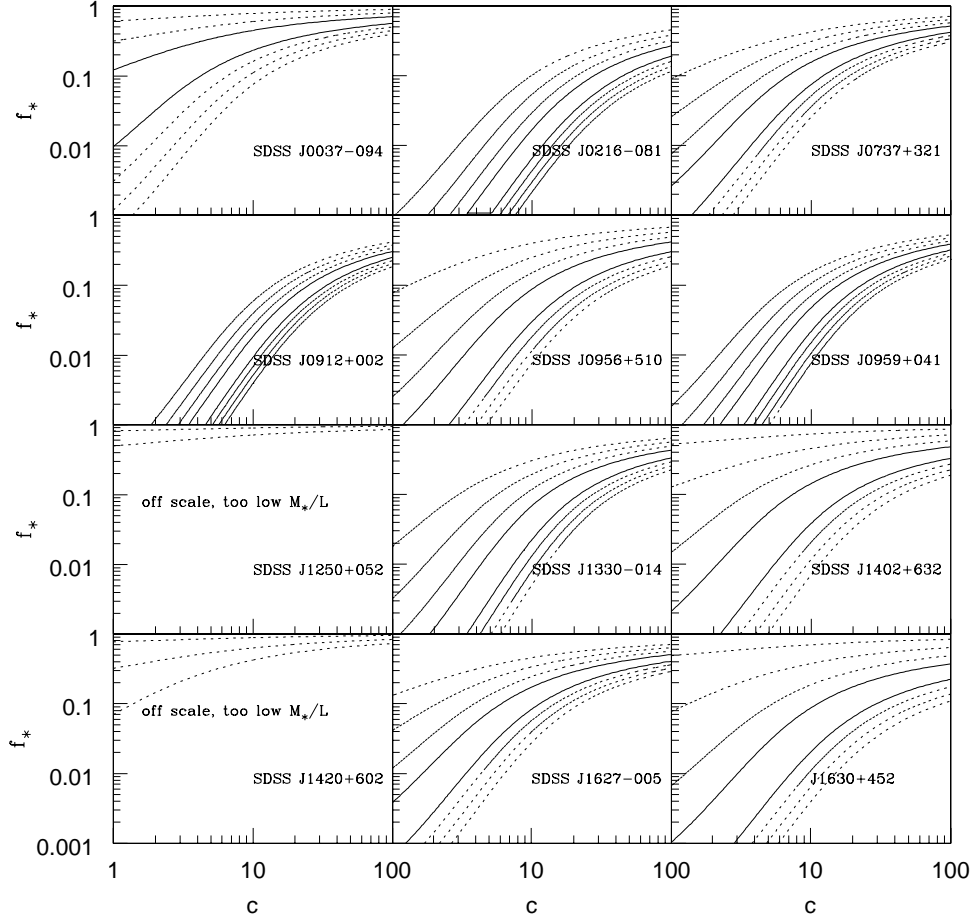
Fig. 2.— The goodness of fit to the mean trend in the stellar mass-to-light ratio as a function of the stellar mass fraction and the concentration c. The solid curves are drawn at $\Delta\chi^2 = 1$ (1σ) for the fit to the mass-to-light ratio and the dotted lines are drawn at $\Delta\chi^2 = 4$, 9 and 16 (2, 3, and 4 σ). The inset text identifies the object. These are the isotropic ($\beta = 0$) adiabatically compressed models that include our estimates of the systematic uncertainties in the stellar dynamical measurements. For these figures, we use the best fit evolution model – the fits would improve if we included the measurement errors in the evolution model.
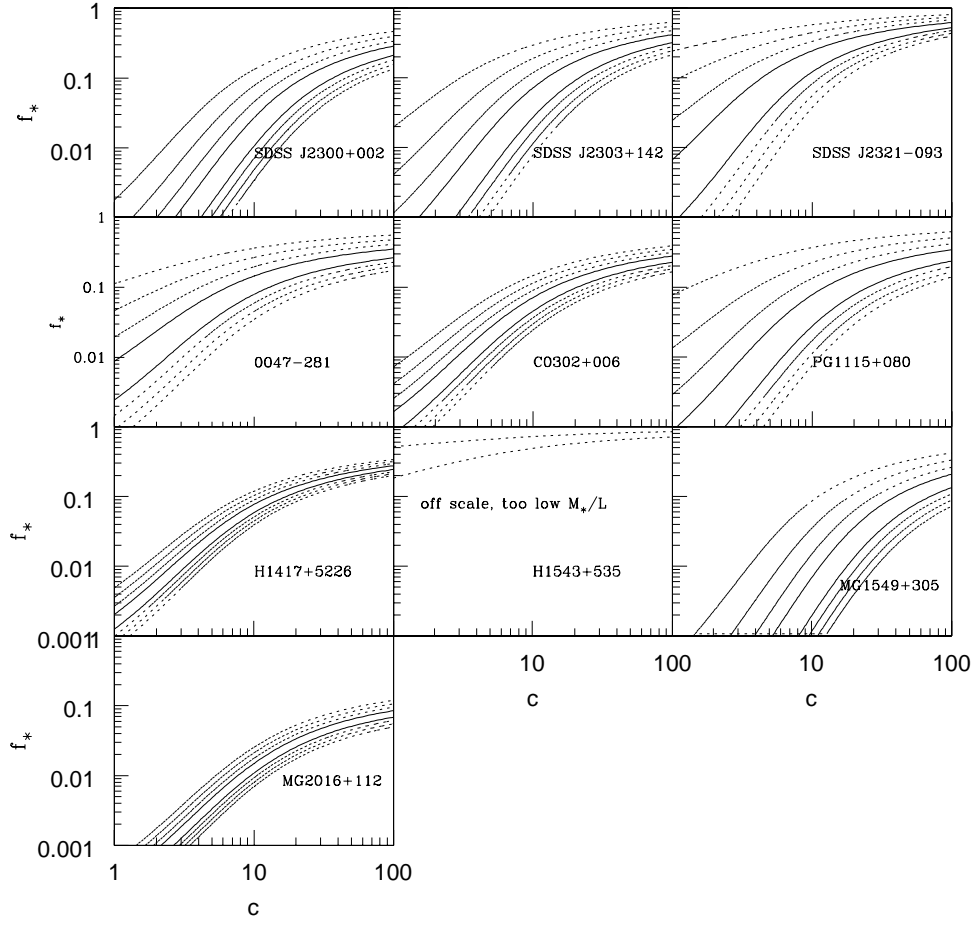
Fig. 2.— continued
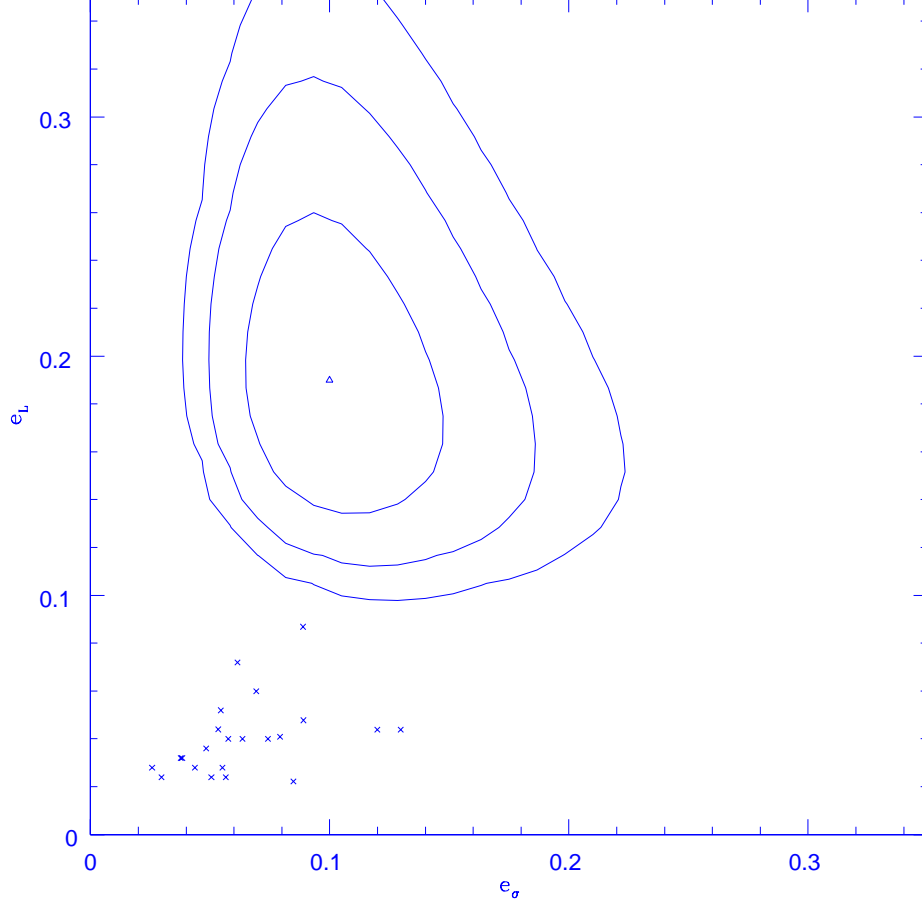
Fig. 3.— The probability distribution of the fractional systematic errors e_σ and e_L in the velocity dispersion and mass-to-light ratio. The contours encompass 68%, 95% and 99.7% of the probability starting from the maximimum likelihood solution indicated by the triangle. The crosses indicate the measurement errors from from Treu et al. (2006) and Koopmans et al. (2006).
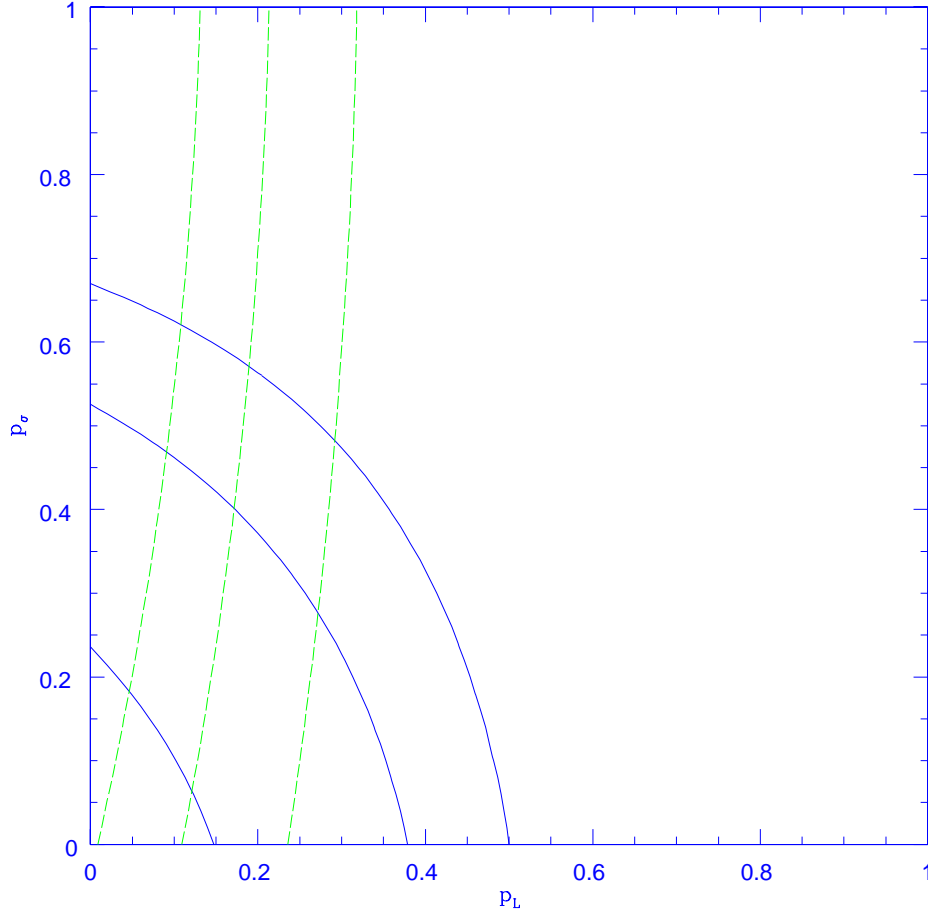
Fig. 4.— The likelihood distributions for the probability that the galaxy sample is homogeneous in its dynamics (p_σ) or its evolution (p_L). The contours encompass 68%, 95% and 99.7% of the probability. The solid contours use the measurement errors for the dynamical uncertainties while the dashed contours include our estimate of the systematic uncertainties in the dynamical measurements. In both cases we used an adiabatically compressed, isotropic $(\beta = 0)$ model.
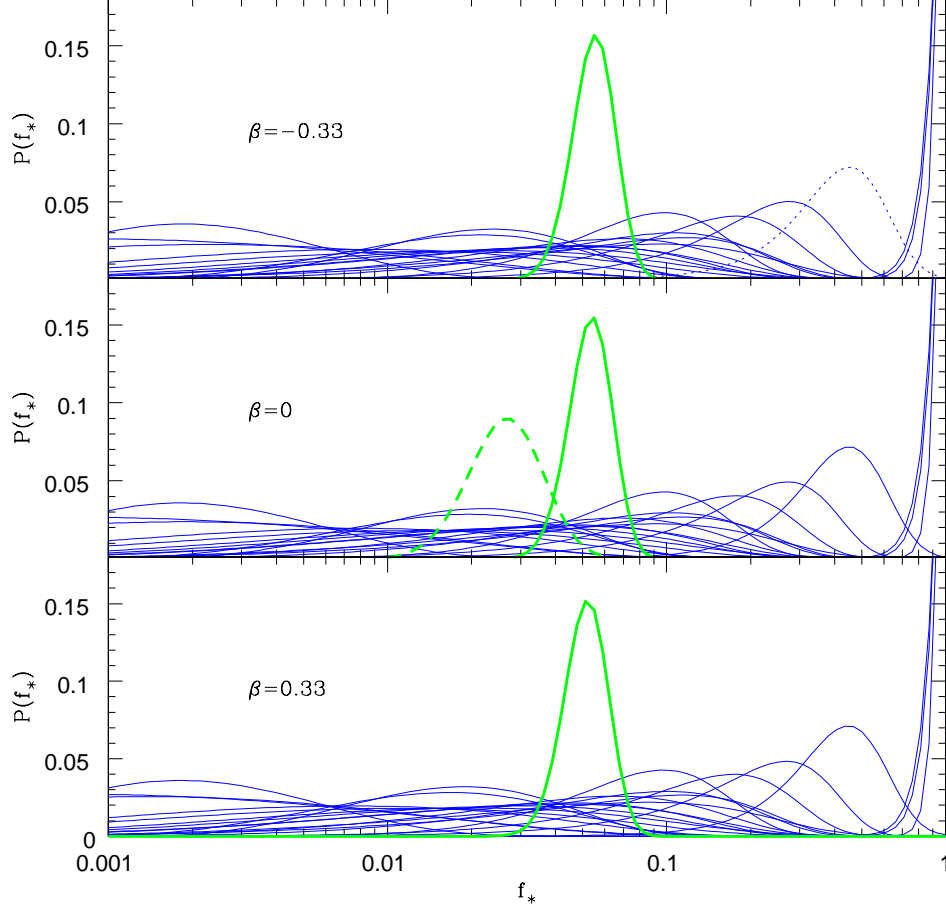
Fig. 5.— The probability distribution for the stellar mass fraction f_* for tangentially anisotropic ($\beta = -0.33$, top panel), isotropic ($\beta = 0$, middle), and radially anisotropic ($\beta = 0.33$, bottom) dynamical models. The thin lines in each panel show the weak constraints found for the individual galaxies, and the thick solid line corresponds to the joint probability from combining the sample. These models are adiabatically compressed using the modified errors and include the fit to the mass-to-light ratios. The thick dashed line in the middle panel shows the effect of not including the adiabatic compressions.
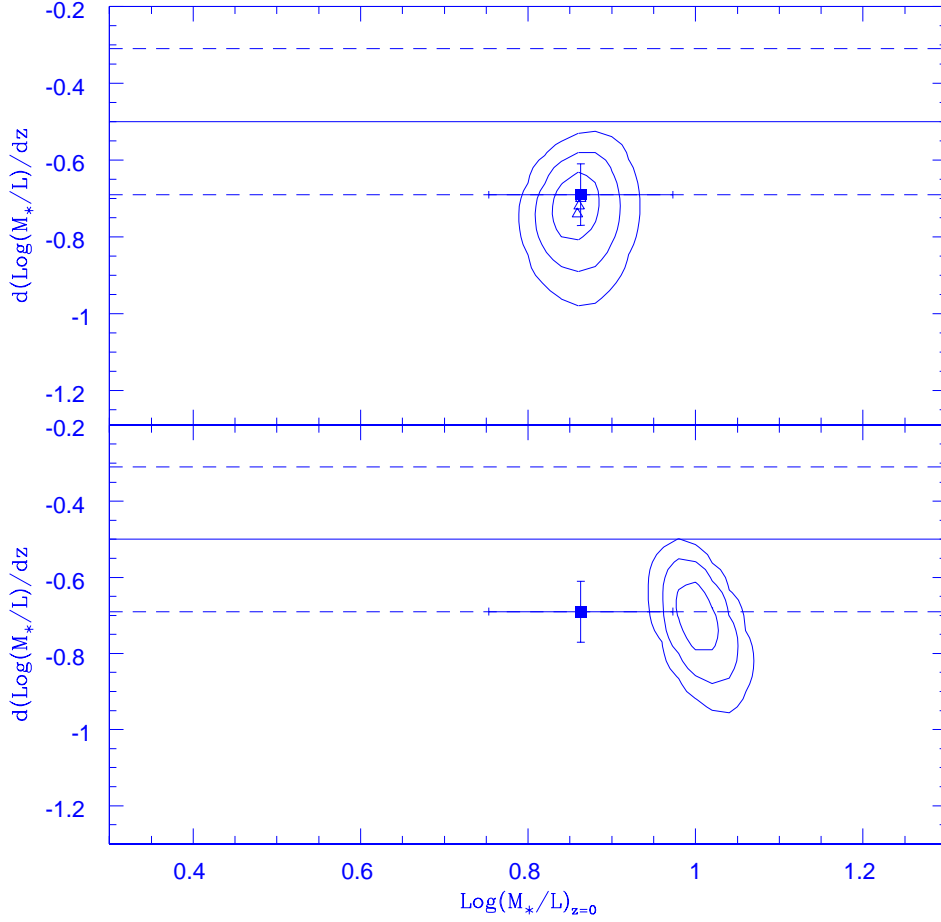
Fig. 6.— The probability distributions for the local mass-to-light ratio $(M_*/L)_0$ and its evolution $d\log(M_*/L)/dz$ in the adiabatically compressed (top) and uncompressed (bottom) models. The contours show the 68%, 95%, and 99.7% enclosed probability contours for the isotropic models. The estimated evolution rate is marginally inconsistent with the estimated of $d\log(M_*/L)/dz = -0.50 \pm 0.19$ from Rusin & Kochanek (2005) which is shown by the horizontal band of solid and dashed lines. The three triangles in each panel show the effect of changing the isotropy on the likelihood peak, with $\beta = -0.33$, $\beta = 0$, and $\beta = 0.33$ as we move from upper left to lower right. The squares with error bars are the results from Treu et al. (2006) for the same galaxies.
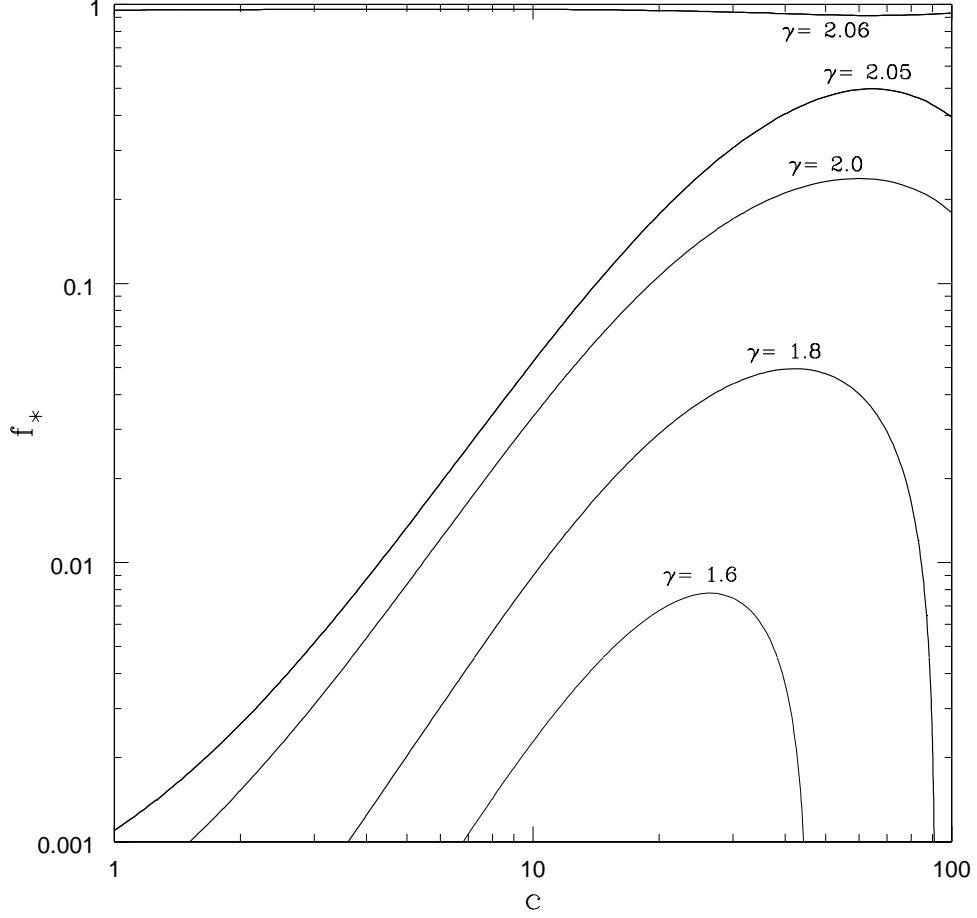
Fig. 7.— The range for the density slope exponent γ, where $\rho \propto r^{-\gamma}$, for the typical lens SDSS J0037–0942. We estimated γ by fitting the projected mass distribution as a power law between $R_e/8$ and R_E. Note that the variation of γ over the physically interesting regime is comparable to the scatter observed by Koopmans et al. (2006) of $1.8 \lesssim \gamma \lesssim 2.3$.